

# Surface Acoustic Waves in Reverse-Biased AlGaIn/GaN Heterostructures

Naoteru Shigekawa, *Member, IEEE*, Kazumi Nishimura, Haruki Yokoyama, and Kohji Hohkawa, *Member, IEEE*

**Abstract**—Properties of surface acoustic waves (SAWs) in reverse-biased AlGaIn/GaN heterostructures on (0001) sapphire substrates were studied by examining the characteristics of SAW filters composed of interdigital Schottky and ohmic contacts. The fundamental and higher frequency SAW signals in measured  $S$ -parameters were attributed to Rayleigh and Sezawa modes, respectively. The onsets of the SAW signals, which were close to the threshold voltage of HEMTs in the vicinities of the respective filters, changed in response to the spatial variation of the threshold voltage. The onset of Sezawa mode was deeper than that of Rayleigh mode, and the difference in onset was larger for longer SAW wavelengths. These results are possibly explained by the change of the input capacitance of interdigital transducers due to the reverse-bias voltages or by the difference in the distribution of SAW energy between the two modes.

**Index Terms**—AlGaIn/GaN, heterostructure, interdigital transducer (IDT), SAW filter, surface acoustic wave (SAW), triple-transit echo (TTE).

## I. INTRODUCTION

**D**UE TO their excellent transport properties as well as large piezoelectricity, group-III nitrides are promising platforms both for high-frequency high-power electron devices and surface-acoustic-wave (SAW) devices [1]. Many authors have explored the possibility of SAW-based devices equipped with interdigital transducers (IDTs), such as SAW filters [2]–[11], ultraviolet sensors [12], and acoustooptic devices [13], on the surfaces of group-III nitride layers. It has been shown that SAWs are excited in AlGaIn/GaN heterostructures with IDTs composed of Ni/Au- or Pt/Ti/Au-based Schottky contacts when bias voltages are applied to the IDTs [14]. The 2-D electron gas (2DEG) formed in the AlGaIn/GaN heterostructures has been successfully applied to the electrodes of IDTs [15].

We previously examined the RF characteristics of SAW filters with IDTs made of interdigital Schottky and ohmic contacts on AlGaIn/GaN heterostructures grown on (0001) sapphire substrates [16]. We observed signals due to SAWs in measured  $S$ -parameters when a reverse-bias voltage  $V_r$  was applied to the IDTs, and we found that the onsets of the SAW signals were close to the threshold voltage  $V_{th}$  of HEMTs that had

been fabricated on the heterostructures in the same process sequence as that for the SAW filters. The results suggested that the electric field due to RF signals applied to IDTs penetrated the GaN layers and excited SAWs in the heterostructures when the 2DEG was depleted. We further showed that SAWs in heterostructures were turned on by applying bias voltages to control gates formed among IDTs [17], which is a demonstration of new functional SAW-based devices.

In group-III nitride layers on (0001) sapphire substrates, due to the difference in elastic properties between the two materials, several SAW modes with different profiles of displacements and different velocities emerge [10]. The velocities of the respective modes depend on the product of the thickness of nitride layers  $H$  and the wavenumber of the SAWs  $k$  ( $= 2\pi/\lambda$  with the SAW wavelength  $\lambda$ ), i.e., the SAW velocities are dispersive. For SAWs propagating along the  $\langle 1\bar{1}00 \rangle$  direction of sapphire substrates, there can occur modes with displacement on sagittal planes, i.e., Rayleigh and Sezawa (higher order Rayleigh) modes, and those with displacement on transversal planes, i.e., Love modes. Among these modes, the Rayleigh and Sezawa modes are intuitively assumed to be electrically excited because the elastic displacements in these modes are coupled to the electric field associated with SAWs.

In this paper, we both experimentally and theoretically investigate the properties of SAWs in reverse-biased AlGaIn/GaN heterostructures on (0001) sapphire substrates. We first describe the process of fabricating SAW filters and their fundamental characteristics—the essential part of which was previously reported [16]. Then, we discuss the features of the measured  $S$ -parameters, such as the spectral shape and the triple-transit echoes (TTEs). In addition, we deeply examine the dependence of the magnitude of the SAW signals on  $V_r$  in terms of the response to change in  $V_{th}$  and the effects of the SAW wavelength. We also analyze the properties of the respective SAW modes by using a theoretical approach, identify modes of the measured SAW signals, and discuss the relation between the distribution of the potential in the heterostructures and the properties of SAWs.

## II. RESULTS

### A. Preparation and Fundamental Characteristics of Samples

We fabricated SAW filters with  $\lambda$  of 2.0, 3.2, 4.0, and 8.0  $\mu\text{m}$  on undoped AlGaIn/GaN heterostructures on (0001) sapphire substrates. The IDTs were made of interdigital Al-based Schottky and Ti/Al-based ohmic contacts. The IDT aperture and the number of finger pairs were  $100\lambda$  and 50, respectively. The separation between the IDTs was  $375\lambda$ . The

Manuscript received February 1, 2008. The review of this paper was arranged by Editor S. Bandyopadhyay.

N. Shigekawa is with the Nippon Telegraph and Telephone (NTT) Photonics Laboratories and the NTT Research and Development Planning Department, NTT Corporation, Atsugi 243-0198, Japan.

K. Nishimura and H. Yokoyama are with the Nippon Telegraph and Telephone (NTT) Photonics Laboratories, NTT Corporation, Atsugi 243-0198, Japan.

K. Hohkawa is with the Kanagawa Institute of Technology, Atsugi 243-0292, Japan.

Digital Object Identifier 10.1109/TED.2008.923565

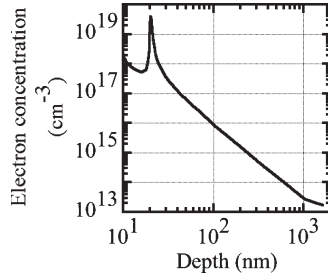


Fig. 1. Profile of the distribution of electrons in heterostructures extracted from the results of capacitance–voltage measurements of Al contacts.

TABLE I  
FUNDAMENTAL CHARACTERISTICS OF SAWS  
OF THE RESPECTIVE FILTERS

$\lambda$ ( $\mu\text{m}$ )	$f_C$ (GHz)	$v_{ph}$ (m/s)	$\Delta f$ (MHz)	$v_{gr}$ (m/s)	Shape of main peak <sup>a</sup>
2.0	1.92	3840	2.4	4080	T
2.0	2.59	5180	2.2	3740	T
3.2	1.25	4000	1.4	3810	T
3.2	1.85	5920	1.8	4900	S
4.0	1.03	4120	1.1	3740	T
4.0	1.67	6680	-	-	S
8.0	0.58	4640	0.57	3880	T

<sup>a</sup>The main peak is composed of a single peak (S), or resolved into two peaks (T).

propagation direction of SAWs was along the  $\langle 1\bar{1}00 \rangle$  direction of sapphire substrates. We simultaneously fabricated HEMTs with 0.5- $\mu\text{m}$  Al gates in the vicinity of the SAW filters.

We measured the capacitance–voltage characteristics of the Al-based Schottky contacts. The extracted profile of the concentration of electrons is shown in Fig. 1. We observed a sharp peak due to the 2DEG at a depth of 20 nm, which was close to the depth of the interface between AlGaIn and GaN layers (nominally 21 nm). The concentration of 2DEG below the Al contacts, which was estimated by integrating the achieved profile of carrier concentration [19], was  $\sim 6 \times 10^{12} \text{ cm}^{-2}$ . The resistivity of the GaN layer was estimated to be  $\sim 10^4 \Omega \cdot \text{cm}$ . Given that the mobility of electrons in undoped bulk GaN is assumed to be  $10^1$ – $10^2 \text{ cm}^2/(\text{V} \cdot \text{s})$ , the electron concentration in the GaN layer was possibly  $10^3$ – $10^{14} \text{ cm}^{-3}$ . Details of the electrical properties of heterostructures and the process for fabricating SAW filters were previously reported [16].

We measured the RF characteristics of the SAW filters at room temperature. Several peaks due to SAWs appeared in the  $|S_{21}|$  spectra when  $V_r$  lower than  $V_{th}$  was applied to the IDTs. We obtained two peaks, namely, fundamental and higher frequency peaks, in each of  $|S_{21}|$  of the 2.0-, 3.2-, and 4.0- $\mu\text{m}$  filters, and one peak, namely, the fundamental peak, in the  $|S_{21}|$  of the 8.0- $\mu\text{m}$  filter. The center frequency  $f_C$  and the phase velocity  $v_{ph}$ , which is defined as  $f_C \times \lambda$ , of each peak are given in Table I.

### B. Spectral Features and Dependence on $V_r$ of $S$ -Parameters

The  $|S_{21}|$  spectra of the 3.2- $\mu\text{m}$  filter around the fundamental ( $f_C = 1.25 \text{ GHz}$ ) and higher frequency (1.85 GHz) peaks at  $V_r$  of  $-10 \text{ V}$  are shown in Fig. 2(a) and (b), respectively. The  $|S_{21}|$  spectrum around 1.25 GHz was resolved into two peaks.

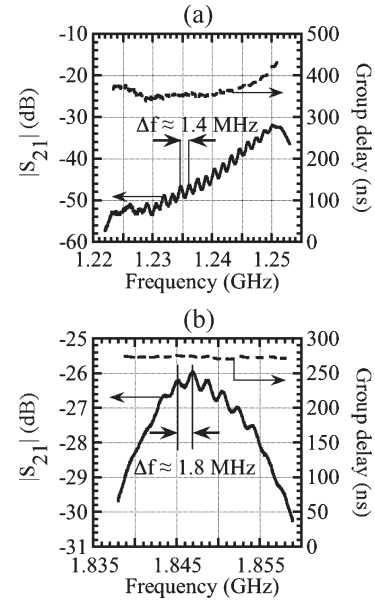


Fig. 2.  $|S_{21}|$  spectra and the group delays at  $V_r$  of  $-10 \text{ V}$  around (a) 1.25 and (b) 1.85 GHz in the 3.2- $\mu\text{m}$  SAW filter.

In contrast, the  $|S_{21}|$  spectrum around 1.85 GHz revealed a single peak.

We found that both the two spectra showed oscillatory features. The ripple frequencies  $\Delta f$  were  $\approx 1.4$  and  $\approx 1.8 \text{ MHz}$  for the 1.25- and 1.85-GHz peaks, respectively. It is noteworthy that the oscillatory features in the 1.25-GHz peak were more marked. The group delays of SAWs, or  $-d[\text{phase of } S_{21}]/d\omega$  with  $\omega$  of the angular velocity, are also shown in the respective figures. We found that the inverse of  $\Delta f$ , i.e., 710 and 560 ns for the 1.25- and 1.85-GHz peaks, respectively, was close to double of the group delay of each  $S_{21}$  signal. The oscillatory features were consequently attributed to the TTEs. The result that the TTEs were more marked and the main peak was resolved into two peaks in the 1.25-GHz signal indicates that this signal is more sensitive to the surface properties, such as the loaded mass at IDTs of AlGaIn/GaN heterostructures, than the 1.85-GHz signal.

Similar to these two spectra, each of the SAW signals of the other filters was either composed of a single peak or resolved into two peaks. Shapes of the respective  $|S_{21}|$  spectra are denoted as “S” (single peak) or “T” (two peaks) in Table I. Oscillatory features due to the TTEs were also identified in other  $|S_{21}|$  spectra, except for the higher frequency spectrum for the 4.0- $\mu\text{m}$  filter. Values of  $\Delta f$  for the respective spectra are also shown in Table I. By assuming that the effective separation between the two IDTs was given by  $375\lambda + 50\lambda = 425\lambda$ , we estimated the group velocity of SAWs  $v_{gr}$  ( $= \Delta f \times 2 \times 425\lambda$ ), which is also shown in the table.

We applied an input RF power of 0 dBm at frequencies of fundamental and higher frequency peaks to the 2.0-, 3.2-, and 4.0- $\mu\text{m}$  filters and measured the transmitted powers. The relation between the transmitted powers and  $V_r$  is shown in Fig. 3(a)–(c). The onsets in the respective curves are denoted by arrows in the figure. It was found that the onsets of the transmitted powers were scattered between  $-2.3$  and  $-2.7 \text{ V}$  and that the differences in onset between the fundamental and

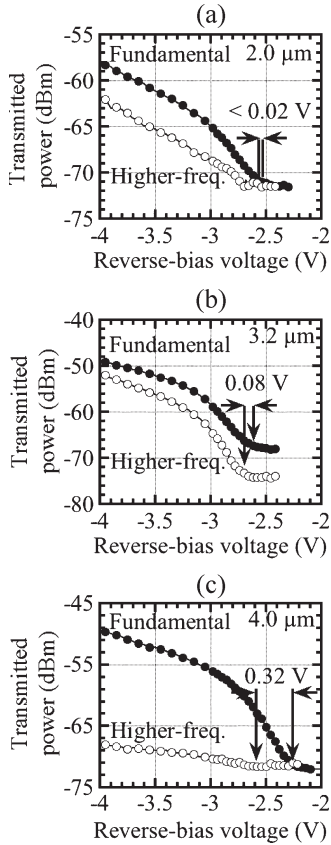


Fig. 3. Relation between the transmitted RF powers through (a) 2.0- $\mu\text{m}$ , (b) 3.2- $\mu\text{m}$ , and (c) 4.0- $\mu\text{m}$  filters and  $V_r$ .

higher frequency signals were  $<0.02$ ,  $0.08$ , and  $\approx 0.32$  V for the 2.0-, 3.2-, and 4.0- $\mu\text{m}$  filters, respectively. It is noteworthy that the onsets of the higher frequency signals were deeper than those of the fundamental signals in the respective filters. In addition, the difference in onset was larger for filters with longer SAW wavelengths.

We compared the dependence of  $|S_{21}|$  at the fundamental and higher frequency peaks on  $V_r$  of the previously discussed 3.2- $\mu\text{m}$  filter (which is referred to as filter A hereafter) with the dependence measured for another 3.2- $\mu\text{m}$  filter (filter B), which had been fabricated and separated from filter A. The results for the two filters are shown in Fig. 4(a) and (b), respectively. As shown in Fig. 4(a),  $|S_{21}|$  of filter A both at the fundamental and higher frequency peaks remained  $-65$  to  $-75$  dB for  $V_r \gtrsim -2.4$  V.  $|S_{21}|$  at both peaks increased when  $V_r$  decreased below  $\approx -2.4$  V. At  $V_r$  of  $-10$  V,  $|S_{21}|$ 's were  $-30.9$  and  $-26.7$  dB at the fundamental and higher frequency peaks, respectively. As shown in Fig. 4(b), behaviors of  $|S_{21}|$  of filter B were similar to those of  $|S_{21}|$  of filter A. The onset of  $|S_{21}|$  was, however,  $\approx -3.2$  V in filter B.

Transfer characteristics at a drain-bias voltage  $V_{\text{DS}}$  of 10 V of HEMTs in the vicinities of filters A and B are shown in Fig. 4(c) and (d), respectively. The maximum transconductances were 170 and 150 mS/mm, respectively. The threshold voltage, which we obtained by linearly extrapolating the transconductance to 0 mS/mm, was found to be  $\approx -2.5$  and  $\approx -3.3$  V for HEMTs in the vicinities of filters A and B, respectively. These values of  $V_{\text{th}}$  are consistent with the result

that the concentration of 2DEG was  $\sim 6 \times 10^{12} \text{ cm}^{-2}$  below the Al contacts (see Fig. 1). It was found that the onsets of  $|S_{21}|$  of filters A and B were close to  $V_{\text{th}}$  of HEMTs in their vicinities, which was consistent with the previous works [16]. More importantly, these results mean that the onsets of SAW signals changed in accordance with the spatially varying electrical characteristics of the AlGaN/GaN heterostructures.

We further extracted the input capacitance  $C_{\text{input}}$  of 3.2- $\mu\text{m}$  IDTs from the  $S$ -parameters for the respective  $V_r$  values. The relation between the input capacitance and  $|S_{21}|$  at the higher frequency peaks is shown for filters A and B in Fig. 4(e). We found that  $C_{\text{input}}$  commonly decreased from  $\approx 8$  to  $\approx 2$  pF when  $|S_{21}|$  increased from  $\approx -55$  to  $\approx -25$  dB. It was unable to precisely estimate  $C_{\text{input}}$  when  $|S_{21}|$  was smaller than  $\approx -55$  dB. Anyhow, this figure shows that all the data points are likely to be placed along a single curve although the relations between  $|S_{21}|$  and  $V_r$  for the respective filters did not coincide with each other, i.e.,  $C_{\text{input}}$  and the magnitude of the SAW signals are in correlation with each other.

### C. Numerical Analysis

We calculated the distribution of the potential  $\phi$  in the reverse-biased 3.2- $\mu\text{m}$  IDTs formed on AlGaN/GaN heterostructures by solving the 2-D Poisson equation. We preset  $V_{\text{th}}$  of HEMTs on the heterostructures to  $\approx -2.5$  V by assuming that a thin  $\delta$ -doped layer was placed at the AlGaN/GaN interfaces. The concentration of the residual impurities in the GaN layer was assumed to be  $10^{14} \text{ cm}^{-3}$ . The variation in the potential due to the change of  $V_r$ , i.e.,  $\partial\phi/\partial V_r$ , is shown for 3.2- $\mu\text{m}$  IDTs at  $V_r = -2, -3, -6, \text{ and } -10$  V in Fig. 5(a)–(d), respectively. We also calculated  $\partial\phi/\partial V_r$  for Schottky-contact-based IDTs on unintentionally doped 2- $\mu\text{m}$ -thick GaN layers. The result is shown in Fig. 5(e).

In cases of  $V_r > V_{\text{th}}$  in AlGaN/GaN heterostructures, as shown in Fig. 5(a), bright areas corresponding to large  $\partial\phi/\partial V_r$  appeared only in regions below the Al Schottky contacts of the top AlGaN layer. The remaining black areas corresponded to  $\partial\phi/\partial V_r = 0$ . This means that the 2DEG at the AlGaN/GaN interface screened the influence of  $V_r$ . On the other hand, for  $V_r < V_{\text{th}}$ , the 2DEG was depleted so that the bright areas were expanded into the GaN layers, as shown in Figs. 5(b)–(d). We confirmed that the vertical extension of the bright areas depended on the concentration of the residual impurities in the GaN layers (not shown). In addition, we found that the 2DEG remained stable in the major part of a region between the Schottky and ohmic contacts even at  $V_r$  of  $-10$  V, so that the potential did not change in the vicinity of the ohmic contacts. In contrast, in the Schottky-contact-based IDTs on unintentionally doped GaN layers, the potential in the GaN layers was modulated in their entire region due to  $V_r$ .

Given that the top AlGaN layer in the heterostructures was far thinner than  $\lambda$ , we assumed that the contribution of the top AlGaN layer to the properties of SAWs was negligibly small and that the properties of SAWs in GaN layers with  $H$  of 2  $\mu\text{m}$  on (0001) sapphire substrates gave a good estimation of the properties of SAWs in the heterostructures. By extremely assuming that no charges existed in the GaN layers, i.e., the

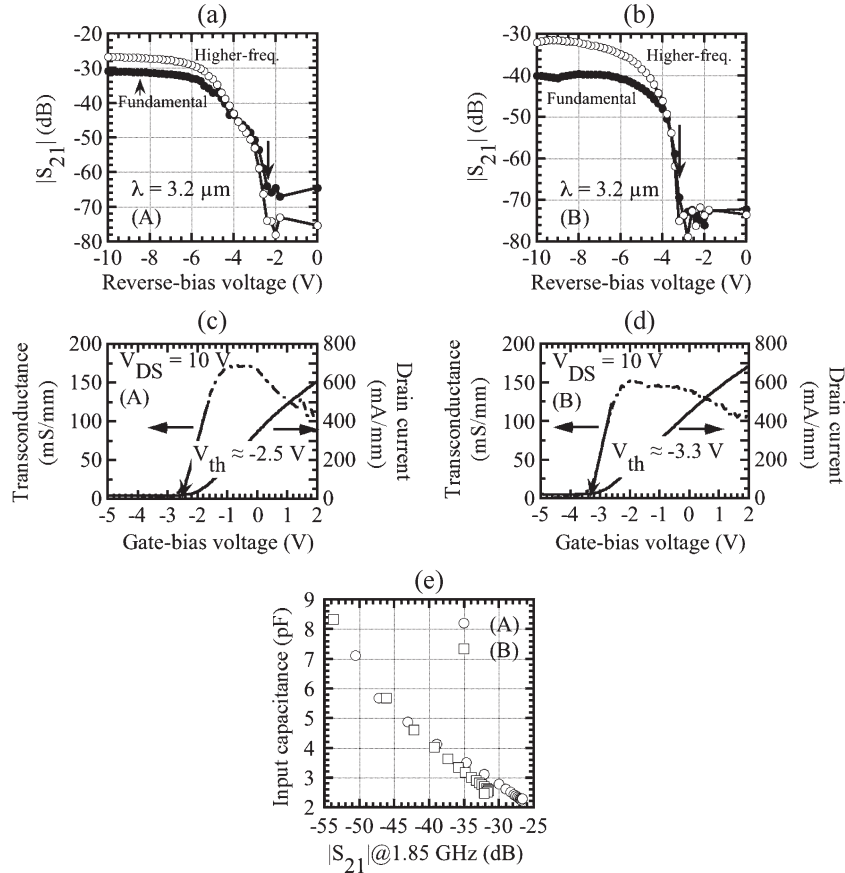


Fig. 4. (a) and (b) Relation between  $|S_{21}|$  at the fundamental and higher frequency peaks and  $V_r$  for 3.2- $\mu\text{m}$  SAW filters A and B. (c) and (d) Transfer characteristics of 0.5- $\mu\text{m}$  HEMTs in the vicinities of filters A and B at  $V_{DS}$  of 10 V. (e) Relation between the input capacitance and  $|S_{21}|$  at the higher frequency  $|S_{21}|$  peak of the 3.2- $\mu\text{m}$  SAW filters A and B.

GaN layers were insulating (insulator model), we calculated the transport characteristics of SAWs, such as their dispersion of velocity and spatial distribution of energy, in GaN layers propagating along the  $\langle 1\bar{1}00 \rangle$  direction of sapphire substrates by using the transfer matrix approach [10], [20]. We used reported values for the mass density  $\rho$ , the elastic constant  $C_{ijkl}$ , the dielectric constant  $\epsilon_{ij}$ , and the piezoelectric coefficient  $e_{ijk}$  for GaN and sapphire [4], [10].

Obtained curves of the dispersion of phase velocity  $v_{ph}$  of Rayleigh (R), Love ( $L_1$  and  $L_2$ ), and Sezawa ( $S_1$ ) modes are shown in Fig. 6(a). The phase velocities given in Table I are also shown. We found that all the phase velocities obtained from the fundamental and higher frequency  $S_{21}$  peaks were close to those on the velocity dispersion curves of the R and  $S_1$  modes, respectively, except the velocity obtained from the higher frequency  $|S_{21}|$  signal of the 4.0- $\mu\text{m}$  filter, which was separated from all of the dispersion curves. This signal might be attributed to the SAW that decays while propagating, or the pseudo-SAW, which was not considered in the present analysis. We found that no experimental data appeared near the dispersion curves of the  $L_1$  and  $L_2$  modes, as was intuitively expected. The fundamental and higher frequency peaks were consequently attributed to the R and  $S_1$  modes, respectively.

We calculated the phase velocities of SAWs in the GaN layers on the other extreme hypothesis that the electrical components of SAWs were identical to zero or that the GaN layers

were metallic (metal model). The difference between the phase velocities of the R mode obtained on these two models is also shown in Fig. 6(a). Although the SAWs cannot be electrically excited on the metal model, it is noteworthy that the difference between the phase velocities obtained in the two extreme models, which is attributed to the piezoelectric stiffness of GaN, was as small as 0.1%–0.4%. Such a small difference is likely to justify the comparison between the measured SAW velocities with those calculated by using the insulator model irrespective of the distribution of the potential in the GaN layers.

We also calculated the group velocity  $v_{gr}$ , which was defined as

$$v_{gr} = \frac{d\omega}{dk} = \frac{d(v_{ph} \times k)}{dk} = v_{ph} + (Hk) \times \frac{dv_{ph}}{d(Hk)}. \quad (1)$$

Curves of the dispersion of  $v_{gr}$  for the R and  $S_1$  modes are shown in Fig. 6(b). The group velocities estimated from  $\Delta f$  values given in Table I are also shown in this figure. We found that the group velocities of the  $S_1$  mode agreed with those extracted from the higher frequency  $|S_{21}|$  peaks, but the group velocities of the R mode were lower than those from the fundamental  $|S_{21}|$  peaks. It is notable, however, that the group velocities of the R mode revealed a minimum at  $Hk \approx 3.5$ , which agreed with the features of the measurements. The systematic deviation in  $v_{gr}$  of the R mode might be related to

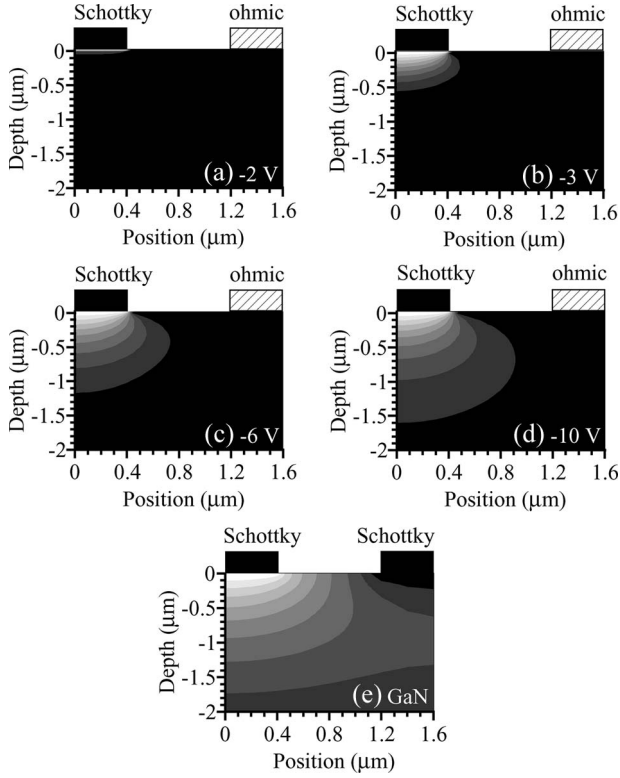


Fig. 5. Variation in the potential of 3.2- $\mu\text{m}$  IDTs on heterostructures due to the change of  $V_r$  at  $V_r$  of (a) -2, (b) -3, (c) -6, and (d) -10 V. (e) Variation in the potential of Schottky-contact-based IDTs on GaN layers.

the possible uncertainty in estimating the effective separation between the IDTs for this mode.

The density of SAW energy  $E_{\text{SAW}}$ , which is the sum of the densities of kinetic, elastic, and electrostatic energies, is expressed as [21]

$$E_{\text{SAW}} = \frac{1}{2}\rho v_i v_i^* + \frac{1}{2}C_{ijkl}\partial_i u_j \partial_k u_l^* + \frac{1}{2}\epsilon_{ij} E_i E_j^* \quad (2)$$

where  $u_i$  and  $E_i$  are the displacement and the electric field along the  $i$ th direction, respectively, and  $v_i$  is the time derivative of displacement ( $v_i = \dot{u}_i$ ). We also defined a depth weighted by the density of SAW energy  $\langle x_3 \rangle$  as

$$\langle x_3 \rangle = \frac{\int_{-\infty}^0 dx_3 x_3 E_{\text{SAW}}}{\int_{-\infty}^0 dx_3 E_{\text{SAW}}} \quad (3)$$

which was assumed to provide us with a measure of the depth of the SAW.

We calculated  $E_{\text{SAW}}$  and  $\langle x_3 \rangle$  on the insulator model. The depth profile of  $E_{\text{SAW}}$  for the R and  $S_1$  modes with  $\lambda$  of 3.2  $\mu\text{m}$  and the curves of the dispersion of  $\langle x_3 \rangle$  for these modes are shown in Fig. 6(c) and (d), respectively. The surface of the GaN layer and the interface between the GaN layer and the sapphire substrate were located at  $x_3 = 0$  and  $-2$   $\mu\text{m}$ , respectively. Note that the energy density was discontinuous at the GaN/sapphire interface because of the difference in  $\rho$ ,  $C_{ijkl}$ , and  $\epsilon_{ij}$  between the two materials. The calculations using the metal model brought out almost the same results.

The SAW energy of each mode was spread over the entire region of the GaN layers and penetrated the sapphire substrates, as is typically seen for the case of  $\lambda$  of 3.2  $\mu\text{m}$ . For this wavelength ( $Hk = 3.9$ ),  $\langle x_3 \rangle$  of the  $S_1$  mode was  $-4.1$   $\mu\text{m}$ , which was the lowest among the  $\langle x_3 \rangle$  values for the wavelengths and modes examined in this paper. Such a low  $\langle x_3 \rangle$  is likely to be consistent with the result that the 1.85-GHz  $|S_{21}|$  signal of the 3.2- $\mu\text{m}$  filter was not sensitive to the surface properties of the filter [Fig. 2(b)].

### III. DISCUSSION

The results of calculating  $\partial\phi/\partial V_r$  shown in Fig. 5(a)–(d) suggest that  $C_{\text{input}}$ , which is determined by the shape of the large  $\partial\phi/\partial V_r$  area in the rudest approximation, decreases as  $V_r$  decreases. The change of  $C_{\text{input}}$  shown in Fig. 4(e) is likely to be explained in this view. Here, we assume that the magnitude of the impedance of the IDTs, which is roughly given by  $1/(2\pi f C_{\text{input}})$ , must be larger than a certain threshold  $Z_{\text{th}}$ , or  $C_{\text{input}}$  must be smaller than  $1/(2\pi f Z_{\text{th}})$ , in order that the electric field exciting SAWs is efficiently induced when the RF signals are applied to the IDTs. On this assumption, the results of calculating  $\partial\phi/\partial V_r$  are likely to be consistent with the following results: 1) that the strong SAW signal was observed when  $V_r$  decreased below  $V_{\text{th}}$  and 2) that the onsets of SAW signals changed in response to the spatial variation of  $V_{\text{th}}$  of HEMTs [Fig. 4(a)–(d)].

We note that  $1/(2\pi f_C Z_{\text{th}})$  at the higher frequency peak was smaller than that at the fundamental peak, and the ratios of  $f_C$  at the higher frequency peak to that at the fundamental peak were larger for longer SAW wavelengths. From Table I, the ratios of  $f_C$  were estimated to be  $(2.59/1.92 =) 1.35$ ,  $(1.85/1.25 =) 1.48$ , and  $(1.67/1.03 =) 1.62$  for  $\lambda = 2.0, 3.2$ , and 4.0  $\mu\text{m}$ , respectively, which suggests that the ratios of  $1/(2\pi f_C Z_{\text{th}})$  at the higher frequency peak to that at the fundamental peak were smaller for longer wavelengths. These arguments might qualitatively explain the experimental result shown in Fig. 3(a)–(c) that the higher frequency SAW signals revealed deeper onsets than the fundamental SAW signals and that the difference in onset was larger for longer SAW wavelengths.

When an RF signal exciting SAWs  $V_0 e^{j\omega t}$  is superimposed on  $V_r$ , the potential in the IDTs  $\phi$  is expressed as

$$\phi(V_r + V_0 e^{j\omega t}) \approx \phi(V_r) + \frac{\partial\phi}{\partial V_r} V_0 e^{j\omega t} \quad (4)$$

which implies that the electric field exciting SAWs in the heterostructures is proportional to the spatial derivative of  $\partial\phi/\partial V_r$ . Fig. 5(a)–(d) consequently indicates that the electric field is induced only within the top AlGaN layer for  $V_r \gtrsim V_{\text{th}}$ , but the field is built up in a wider part of heterostructures when  $V_r$  decreases below  $V_{\text{th}}$ . By assuming that SAWs are more efficiently excited when the overlap of the electric field and the profile of displacements of SAWs is larger, i.e., when the penetration depth of  $\partial\phi/\partial V_r$  is closer to the depth characterizing the distribution of the SAW energy, the results shown in Fig. 3(a)–(c) might be alternatively explained by the calculation of distribution of the SAW energy, which indicated that the  $S_1$  mode was distributed more deeply than the R mode and that the

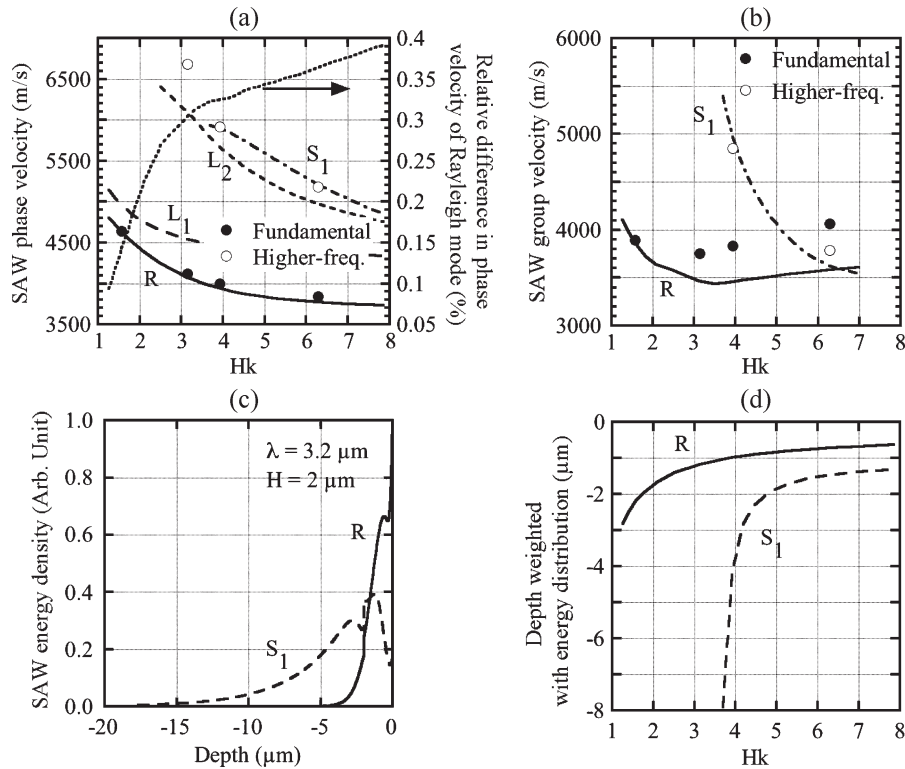


Fig. 6. Transport characteristics of SAWs propagating along the  $\langle 1\bar{1}00 \rangle$  of sapphire in GaN layers on (0001) sapphire substrates calculated by using the insulator model. (a) Dispersion curves of phase velocity for the R,  $L_1$ ,  $L_2$ , and  $S_1$  modes. The results of measurements and the difference between the phase velocities of R mode calculated by using the insulator and metal models are also shown. (b) Dispersion curves of group velocity for the R and  $S_1$  modes. The velocities extracted from the TTE characteristics are also shown. (c) Depth profile of energy density for the R and  $S_1$  modes with  $\lambda = 3.2 \mu\text{m}$ . (d) Dispersion curves of the depth weighted by the density of energy for the R and  $S_1$  modes.

difference in depth between the two modes increased when  $Hk$  decreased, i.e.,  $\lambda$  increased [Fig. 6(d)].

We should note that the semiconducting and piezoelectric properties of group-III nitrides were not simultaneously considered in the present analysis, which kept the discussion of the exciting and detecting characteristics of SAWs qualitative. To precisely grasp the exciting, transport, and detecting characteristics of SAWs in reverse-biased AlGaIn/GaN heterostructures, we have to solve the Poisson equation, the stress equations of motion, and the constitutive equations of SAWs in self-consistent manners, estimate the input capacitance, the SAW velocity, and the electromechanical coupling coefficient, and determine the electric-to-acoustic power transfer efficiency  $p_{13}$  [22]. The establishment of such process should be targeted in the next stage of the course of study of SAW properties in group-III nitrides. From practical viewpoints, irrespective of the mechanism bringing out the difference in onset between the R and  $S_1$  modes, a smaller difference is assumed to be preferable since the GaN layers with smaller concentrations of residual impurities in their deep inside are sought for in order to realize electron devices with higher breakdown voltages.

#### IV. CONCLUSION

We examined the properties of the SAWs in reverse-biased AlGaIn/GaN heterostructures grown on (0001) sapphire substrates by investigating the characteristics of SAW filters composed of IDTs made of interdigital Schottky and ohmic contacts. We observed the fundamental and higher frequency

SAW signals in  $S$ -parameters of filters, which were attributed to Rayleigh and Sezawa modes, respectively. The features of the respective SAW peaks in the  $|S_{21}|$  spectra, which are related to the sensitivity to the surface properties, were found to be in correlation with the depth weighted by the density of SAW energy. Measurements of the relation between  $|S_{21}|$  due to SAWs and the reverse-bias voltage applied to the Schottky contacts showed that the onsets of  $|S_{21}|$ , which were close to the threshold voltages of HEMTs in the vicinities of the respective filters, changed in accordance with the spatially varying threshold voltage. We also found that the onset of Sezawa mode was deeper than that of Rayleigh mode and that the difference in onset was larger for longer SAW wavelengths. These results may be explained by the change of the input capacitance of IDTs due to the reverse-bias voltages or by the difference in the distribution of the energy of SAWs between the Rayleigh and Sezawa modes.

#### ACKNOWLEDGMENT

The authors would like to thank T. Makimura and K. Shiojima for their advice in device fabrication and T. Kobayashi and T. Enoki for their encouragement.

#### REFERENCES

- [1] O. Ambacher, "Growth and applications of Group III-nitrides," *J. Phys. D, Appl. Phys.*, vol. 31, no. 20, pp. 2653–2710, Oct. 1998.
- [2] C. Deger, E. Born, H. Angere, O. Ambacher, M. Stutzmann, J. Hornsteiner, E. Riha, and G. Fischerauer, "Sound velocity of

- Al<sub>x</sub>Ga<sub>1-x</sub>N thin films obtained by surface acoustic-wave measurements," *Appl. Phys. Lett.*, vol. 72, no. 19, pp. 2400–2402, May 1998.
- [3] S.-H. Lee, H.-H. Jeong, S.-B. Bae, H.-C. Choi, J.-H. Lee, and Y.-H. Lee, "Epitaxially grown GaN thin-film SAW filter with high velocity and low insertion loss," *IEEE Trans. Electron Devices*, vol. 48, no. 3, pp. 524–529, Mar. 2001.
- [4] Y. Takagaki, P. V. Santos, E. Wiebicke, O. Brandt, H.-P. Schönherr, and K. H. Ploog, "Guided propagation of surface acoustic waves in AlN and GaN films grown on 4H-SiC(0001) substrates," *Phys. Rev. B, Condens. Matter*, vol. 66, no. 15, p. 155 439, Oct. 2002.
- [5] R. Rimeika, D. Ciplys, M. S. Shur, R. Gaska, M. A. Khan, and J. Yang, "Electromechanical coupling coefficient for surface acoustic waves in GaN-on-sapphire," *Phys. Stat. Sol. (B)*, vol. 234, no. 3, pp. 897–900, Dec. 2002.
- [6] K. H. Choi, H. J. Kim, S. J. Chung, J. Y. Kim, T. K. Lee, and Y. J. Kim, "Experimental and theoretical characterization of the surface acoustic wave propagation properties of GaN epitaxial layers on c-plane sapphire," *J. Mater. Res.*, vol. 18, no. 5, pp. 1157–1161, May 2003.
- [7] J. Camacho, P. V. Santos, F. Alsina, M. Ramsteiner, K. H. Ploog, A. Cantarero, H. Obloh, and J. Wagner, "Modulation of the electronic properties of GaN films by surface acoustic waves," *J. Appl. Phys.*, vol. 94, no. 3, pp. 1892–1897, Aug. 2003.
- [8] K. Nishimura, N. Shigekawa, H. Yokoyama, M. Hiroki, and K. Hohkawa, "SAW characteristics of GaN layers with surfaces exposed by dry etching," *IEICE Electron. Exp.*, vol. 2, no. 19, pp. 501–505, Oct. 2005.
- [9] N. Shigekawa, K. Nishimura, H. Yokoyama, and K. Hohkawa, "Side-gate effects on transfer characteristics in GaN-based transversal filters," *Appl. Phys. Lett.*, vol. 87, no. 8, p. 084 102, Aug. 2005.
- [10] J. Pedrós, F. Calle, J. Grajal, R. J. J. Riobóo, Y. Takagaki, K. H. Ploog, and Z. Bougrioua, "Anisotropy-induced polarization mixture of surface acoustic waves in GaN/c-sapphire heterostructures," *Phys. Rev. B, Condens. Matter*, vol. 72, no. 7, p. 075 306, Aug. 2005.
- [11] K. Nishimura, N. Shigekawa, H. Yokoyama, and K. Hohkawa, "SAW characteristics of GaN with n<sup>+</sup>-GaN IDTs," *Electron. Lett.*, vol. 42, no. 1, pp. 62–63, Jan. 2006.
- [12] D. Ciplys, R. Rimeika, M. S. Shur, S. Romyantsev, R. Gaska, A. Sereika, J. Yang, and M. A. Khan, "Visible-blind photoresponse of GaN-based surface acoustic wave oscillator," *Appl. Phys. Lett.*, vol. 80, no. 11, pp. 2020–2022, Mar. 2002.
- [13] G. Bu, M. S. Shur, D. Čiplys, R. Rimeika, R. Gaska, and Q. Fareed, "Guided-wave acousto-optic diffraction in Al<sub>x</sub>Ga<sub>1-x</sub>N epitaxial layers," *Appl. Phys. Lett.*, vol. 85, no. 12, pp. 2157–2159, Sep. 2004.
- [14] F. Calle, J. Grajal, and J. Pedrós, "Active SAW devices on 2DEG heterostructures," *Electron. Lett.*, vol. 40, no. 21, pp. 1384–1386, Oct. 2004.
- [15] K.-Y. Wong, W. Tang, K. M. Lau, and K. J. Chen, "Surface acoustic wave device on AlGa<sub>x</sub>/Ga<sub>1-x</sub>N heterostructure using two-dimensional electron gas interdigital transducers," *Appl. Phys. Lett.*, vol. 90, no. 21, p. 213 506, May 2007.
- [16] N. Shigekawa, K. Nishimura, T. Suemitsu, H. Yokoyama, and K. Hohkawa, "SAW filters composed of interdigital schottky and ohmic contacts on AlGa<sub>x</sub>/Ga<sub>1-x</sub>N heterostructures," *IEEE Electron Device Lett.*, vol. 28, no. 2, pp. 90–92, Feb. 2007.
- [17] N. Shigekawa, K. Nishimura, T. Suemitsu, H. Yokoyama, and K. Hohkawa, "Interdigital transducers with control gates on AlGa<sub>x</sub>/Ga<sub>1-x</sub>N heterostructures," *Appl. Phys. Lett.*, vol. 89, no. 3, p. 033 501, Jul. 2006.
- [18] K. A. Rickert, A. B. Ellis, J. K. Kim, J.-L. Lee, F. J. Himpfel, F. Dwikusuma, and T. F. Kuech, "X-ray photoemission determination of the Schottky barrier height of metal contacts to n-GaN and p-GaN," *J. Appl. Phys.*, vol. 92, no. 11, pp. 6671–6678, Dec. 2002.
- [19] O. Ambacher, J. Smart, J. R. Shealy, N. G. Weimann, K. Chu, M. Murphy, W. J. Schaff, L. F. Eastman, R. Dimitrov, L. Wittmer, M. Stutzmann, W. Rieger, and J. Hilsenbeck, "Two-dimensional electron gases induced by spontaneous and piezoelectric polarization charges in N- and Ga-face AlGa<sub>x</sub>/Ga<sub>1-x</sub>N heterostructures," *J. Appl. Phys.*, vol. 85, no. 6, pp. 3222–3233, Mar. 1999.
- [20] E. L. Adler, "Matrix methods applied to acoustic waves in multilayers," *IEEE Trans. Ultrason., Ferroelectr., Freq. Control*, vol. 37, no. 6, pp. 485–490, Nov. 1990.
- [21] H. F. Tiersten, *Linear Piezoelectric Plate Vibrations*. New York: Plenum, 1969.
- [22] H. M. Gerard, "Principles of Surface Wave Filter Design," in *Acoustic Surface Waves*. New York: Springer-Verlag, 1978.



**Naoteru Shigekawa** (M'01) received the B.S., M.S., and Ph.D. degrees in physics from the University of Tokyo, Tokyo, Japan, in 1984, 1986, and 1993, respectively.

He was with the Atsugi Electrical Communication Laboratories, Nippon Telegraph and Telephone (NTT) Corporation, Atsugi, Japan, in 1986, and was engaged in research on hot-carrier transport in III–V compound-semiconductor heterostructures. From 1993 to 1994, he was a Visiting Scientist with the Department of Physics, University of Nottingham, Nottingham, U.K., where he worked on resonant-tunnelling heterojunction bipolar transistors. He is currently with the NTT Photonics Laboratories, NTT Corporation. He is also with the NTT Research and Development Planning Department, where he has been engaged in the process of creating new business from achievements of NTT's R&D activities. His current research interests include transport properties in compound-semiconductor heterostructures and electron devices.

Dr. Shigekawa is a member of the Physical Society of Japan, the Japan Society of Applied Physics, the American Physical Society, and the Institute of Physics.



**Kazumi Nishimura** was born in Kyoto, Japan, on January 28, 1961. He received the B.E., M.E., and D.E. degrees from Tohoku University, Sendai, Japan, in 1984, 1987, and 1999, respectively.

In 1987, he was with the Nippon Telegraph and Telephone (NTT) Atsugi Electrical Communication Laboratories, Atsugi, Japan. He is currently with the NTT Photonics Laboratories, NTT Corporation. He has been engaged in the research and development of device design and process technology of compound-semiconductor devices.

Dr. Nishimura is a member of the Institute of Electronics, Information and Communication Engineers of Japan and the Japan Society of Applied Physics.



**Haruki Yokoyama** was born in Kochi, Japan, on March 7, 1965. He received the B.S. and M.S. degrees in electrical engineering from Hiroshima University, Hiroshima, Japan, in 1987 and 1989, respectively, and the Ph.D. degree in applied physics from Tohoku University, Sendai, Japan, in 1996.

He was with the Nippon Telegraph and Telephone (NTT) LSI Laboratories, Kanagawa, Japan, in 1989. Since then, he has been engaged in the research and development work on epitaxial growth technologies of III–V compound semiconductors using metal–organic vapor phase epitaxy. He is currently with the NTT Photonics Laboratories, NTT Corporation, Atsugi, Japan.

Dr. Yokoyama is a member of the Japan Society of Applied Physics.



**Kohji Hohkawa** (A'93–M'94) received the B.E., M.E., and D.E. degrees in electrical engineering from Osaka University, Osaka, Japan, in 1969, 1971, and 1980, respectively.

In 1971, he was with the Electrical Communication Laboratories, Nippon Telegraph and Telephone Public Corporation, where he engaged in the research and development of piezoelectric devices, including surface-acoustic-wave (SAW) devices in early 1970s. He also engaged in the research works on superconducting devices, including Josephson junction logic devices and vortex memory devices, and the early stages of nano-electronic devices. He furthermore engaged in the research and development of ultrahigh-speed optical fiber transmission systems, namely, F10G. Since 1993, he has been with the Kanagawa Institute of Technology, Atsugi, Japan, where he is currently a Professor engaging in research works on solid-state devices, including SAW, superconductor, semiconductor, and MEMS devices.

Dr. Hohkawa is a member of the Japanese Society of Applied Physics and the Institute of Electronics, Information and Communication Engineers, Japan.